



LAWRENCE
LIVERMORE
NATIONAL
LABORATORY

Ultrafast K-(alpha) X-ray Thomson Scattering from Shock Compressed Lithium Hydride

A. L. Kritcher, P. Neumayer, J. Castor, T. Doeppner, R.
W. Falcone, O. L. Landen, H. J. Lee, R. W. Lee, B.
Holst, R. Redmer, E. C. Morse, A. Ng, S. Pollaine, D.
Price, S. H. Glenzer

December 19, 2008

Physics of Plasmas

Disclaimer

This document was prepared as an account of work sponsored by an agency of the United States government. Neither the United States government nor Lawrence Livermore National Security, LLC, nor any of their employees makes any warranty, expressed or implied, or assumes any legal liability or responsibility for the accuracy, completeness, or usefulness of any information, apparatus, product, or process disclosed, or represents that its use would not infringe privately owned rights. Reference herein to any specific commercial product, process, or service by trade name, trademark, manufacturer, or otherwise does not necessarily constitute or imply its endorsement, recommendation, or favoring by the United States government or Lawrence Livermore National Security, LLC. The views and opinions of authors expressed herein do not necessarily state or reflect those of the United States government or Lawrence Livermore National Security, LLC, and shall not be used for advertising or product endorsement purposes.

Ultrafast K- α X-ray Thomson Scattering from Shock Compressed Lithium Hydride

A. L. Kritcher[†], P. Neumayer^{*}, J. Castor^{*}, T. Döppner^{*}, R. W. Falcone[‡], O. L. Landen[‡], H. J. Lee[‡], R. W. Lee^{*‡}, B. Holst^{**}, R. Redmer^{**}, E. C. Morse[†], A. Ng^{*}, S. Pollaine^{*}, D. Price^{*}, and S. H. Glenzer^{*}

^{*}L-399, Lawrence Livermore National Laboratory, P.O. Box 808, Livermore, CA 94551, USA

[†] Nuclear Engineering Department, University of California Berkeley, Berkeley, CA 94709

[‡] Physics Department, University of California Berkeley, Berkeley, CA 94709 and

^{**} Universität Rostock, Institut für Physik, D-18051 Rostock, Germany

(Dated: December 18, 2008)

Spectrally and temporally resolved x ray Thomson scattering using ultrafast Ti K- α x-rays has provided experimental validation for modeling of the compression and heating of shocked matter. The coalescence of two shocks launched into a solid density LiH target by a shaped 6 nanosecond heater beam was observed from rapid heating to temperatures of 2.2 eV, enabling tests of shock timing models. Here, the temperature evolution of the target at various times during shock progression was characterized from the intensity of the elastic scattering component. The observation of scattering from plasmons, electron plasma oscillations, at shock coalescence indicates a transition to a dense metallic plasma state in LiH. From the frequency shift of the measured plasmon feature the electron density was directly determined with high accuracy, providing a material compression of a factor of three times solid density. The quality of data achieved in these experiments demonstrates the capability for single-shot dynamic characterization of dense shock compressed matter. The conditions probed in this experiment are relevant for the study of the physics of planetary formation and to characterize inertial confinement fusion targets for experiments such as on the National Ignition Facility (NIF), LLNL.

Keywords: K-alpha X-ray Scattering, Thomson Scattering, Compton Scattering, Shock Compression

INTRODUCTION

Material conditions in the high-energy-density-physics regime relevant for the study of planetary formation [1] and the modeling of planetary composition[2] can be produced and studied in the laboratory using high powered lasers that shock compress material to pressures greater than > 1 Mbar. Current experiments to measure the equation of state (EOS) and effects of shock waves on matter for light elements [3–5] are designed to investigate the physics of planetary formation and the effects of solar nebula shocks [6]. The study of shock wave heating in light elements under high pressure conditions is also important for inertial confinement fusion experiments [7] such as on the future National Ignition Facility (NIF) [8] at the Lawrence Livermore National Laboratory (LLNL) where deuterium-tritium filled capsules will be compressed to densities greater than 1000 times solid density using a sequence of coalescing shock waves.

In this experiment, we have directly measured the thermodynamic properties and structure factors of shocked matter [9]. These experiments have become recently possible with the use of high-energy (300 J) petawatt-class ultra-short pulse lasers to produce powerful x-ray probes [10]. Here, we shock compress solid density LiH targets with an energetic, shaped, 6 nanosecond laser beam and use spectrally-resolved x-ray Thomson scattering [11] to measure the material conditions. The shaped heater beam drove two coalescing shocks into a solid density LiH target to shock compress the material. Experimental data show scattering from plasmons, electron plasma

waves, at shock coalescence indicating a transition to the dense metallic plasma state in LiH. Here, an electron density of $1.7 \times 10^{23} \text{cm}^{-3}$ was directly determined from the frequency shift of the plasmon peak. An ionization state of $Z^* = 1.0 \pm 10\%$ was determined from the shape of the bound-free scattering feature, yielding a material compression of three times solid density with known electron density.

Measurement of the elastic scattering feature intensity provided the temperature at various times during shock compression from dependency on the ion-ion structure factor. Rapid heating to temperatures of 2.2 eV indicates shock coalescence, allowing tests of models that predict shock timing. For example, radiation-hydrodynamic modeling of the target conditions were in agreement with experimental data; while the range of temperatures measured during shock compression agrees with calculations using a quotidian [12] equation-of-state (QEOS), the shock coalescence time is matched using Sesame [13] EOS tables.

Previous x-ray scattering experiments have allowed characterization of dense matter, $n_e > 3 \times 10^{21} \text{cm}^{-3}$, that cannot be probed using the well established technique of optical Thomson scattering [14]. In these experiments, spectrally resolved x-ray scattering in the collective and non-collective regimes using He- α and Ly- α sources [11, 15] provided information on the temperatures and densities of solid-density plasmas enabling future measurements of the equation of state, phase transitions, and the compressibility of dense matter. The temporal resolution of 100 ps for these He- α and Ly- α sources, obtained with gated microchannelplate detec-

tors, was sufficient for measuring the conditions in radiatively heated matter. However, for the full characterization of strong shocks in dense matter, an x-ray source that provides picosecond temporal resolution is advantageous.

In this work we provide the first successful K- α x-ray scattering measurements from shock compressed matter [9] and discuss the experimental constraints and data analysis in greater detail. This x-ray probe has a temporal resolution of ~ 10 ps [17], that can provide a snapshot of the material conditions for dynamically shocked systems. In addition, the Ti K- α line has a small bandwidth of $\Delta E/E=0.3\%$ and no satellites on the red wing, in contrast to previously used Ly- α and He- α sources with $\Delta E/E > 1\%$, enabling high resolution of the down-scattered plasmon in the collective scattering regime. High quality data taken in these laser experiments, with $\sim 10^{12}$ probe photons on target, demonstrates the capability of K- α x-ray scattering for single shot characterization.

In section II we will discuss the experimental constraints for x-ray Thomson scattering from dense plasmas in the collective regime, accessed in this experiment, to observe the collective behavior of the electrons. Section III will include the experimental set-up, instrumentation, and design considerations such as source intensity and scattering geometry. The experimental data and discussion are presented in section IV with a sensitivity analysis of the experimental data to plasma parameters such as density, temperature, and ionization state. Here, the transition to the metallic state in LiH is discussed. Section V will present the conclusions and the future outlook.

X-RAY THOMSON SCATTERING

In this experiment, x-rays are scattered from free, weakly bound, and tightly bound electrons. Here, the tightly and weakly bound electrons have ionization potentials greater than and less than the Compton energy, respectively. For accurate measurement of electron density from first principles, we probe the collective scattering regime. Scattering in the collective regime results in the observation of a resonance from plasma oscillations [11], i.e., plasmon modes, while scattering in the non-collective regime is the scattering of x-rays by individual electrons, i.e., the Compton regime [17]. In collective scattering, the frequency shift of the plasmon feature directly yields the electron density.

The Thomson scattering cross-section can be expressed using the total structure factor, $S(\mathbf{k}, \omega)$ [18, 19]

$$\frac{d^2\sigma_T}{d\Omega d\omega} = \sigma_T \frac{k_1}{k_0} S(\mathbf{k}, \omega) \quad (1)$$

where σ_T is the Thomson scattering cross-section for a range of frequencies and solid angles, and k_1 and k_0 are the scattered and incident radiation wave vectors, respectively. The total structure factor is given by [18, 19]

$$S(\mathbf{k}, \omega) = |f_I(k) + q(k)|^2 S_{ii}(k, \omega) + Z_f S_{ee}^o(k, \omega) + Z_c \int S_{ce}(k, \omega - \omega') S_s(k, \omega') d\omega' \quad (2)$$

where Z_f and Z_c are the effective free and core electron states of the system. The first term in Eq. (2) results from scattering from electrons that dynamically follow the ion motion, where $S_{ii}(k, \omega)$ is the ion-ion density correlation function, $f_I(k)$, the ion-ion form factor, accounts for scattering from core electrons, and $q(k)$ describes scattering from a screening cloud of valance electrons encompassing the ion. The second term accounts for scattering from free de-localized electrons that do not follow ion motion, where $S_{ee}^o(k, \omega)$ is the electron-electron density correlation function. The third term describes inelastic scattering resulting from bound-free transitions to the continuum of core electrons within an ion, $S_{ce}(k, \omega)$. Here, $S_s(k, \omega)$ represents a modulation due to the self-motion of the ions.

The collective scattering regime can be accessed with appropriate choice of probe energy and scattering angle. The scattering parameter α distinguishes the collective scattering regime from the non-collective regime where

$$\alpha = \frac{1}{k\lambda_S} = \frac{\lambda}{2\pi\lambda_S} \quad (3)$$

the parameters k and λ are the wavevector and wavelength probed by the scattering experiment, and λ_S is the screening length of the plasma, the length at which local electric fields are screened out by mobile charge carriers, i.e., electrons. In the collective regime ($\alpha > 1$), plasmon modes [11] are accessed by probing plasma scale lengths larger than the plasma screening length. In the non-collective regime ($\alpha < 1$), plasma scale lengths smaller than the screening length are probed and information on the individual electrons is obtained [17].

For a degenerate system, the plasma screening length can be approximated by the Thomas-Fermi length [20], λ_{TF}

$$\lambda_{TF} = \left(\frac{\pi\epsilon_0\hbar^2}{m_e e^2} \left(\frac{\pi}{3n_e} \right)^{1/3} \right)^{1/2} \quad (4)$$

where, n_e is the electron density, m_e and e are the mass and charge of the electron, respectively, and $h = 2\pi\hbar$ is Planck's constant. For a classical plasma, λ_S is the

Debye length, $\lambda_D = (\epsilon_0 k T_e / n_e e^2)^{1/2}$ where ϵ_0 is the permittivity of free space, k is the Boltzmann constant, T_e is the electron temperature, and n_e is the electron density. For weakly degenerate plasmas, calculating the Debye length at an effective temperature results in a smooth interpolation between the degenerate and classical plasma regimes. [21, 22].

For small energy transfers of incident x-ray energy to the electrons ($k_0 \approx k_s$ where $k_0 = 2\pi E_0 / hc$ and k_s is the scattered wavevector), the magnitude of the scattering vector, \mathbf{k} , can be approximated by

$$k = |\mathbf{k}| = 2k_0 \sin(\theta/2) = 4\pi \frac{E_0}{hc} \sin(\theta/2). \quad (5)$$

Thus, the scattering parameter, α , is dependent on the scattering angle, θ , the energy of the probe radiation, E_0 , through the scattering vector, and the plasma parameters, T_e and n_e , through the screening length. For example, to access collective scattering in a degenerate solid-density plasma with $T_e = 2$ eV and $n_e = 2 \times 10^{23} \text{cm}^{-3}$, $\alpha > 1$ for $\theta = 40^\circ$ and x-ray energies $E_0 \leq 5$ keV. For these conditions, higher x-ray probe energies, $E_0 > 5$ keV will result in non-collective scattering.

In collective scattering, the spectrum includes collective electron oscillation peaks, i.e. plasmons up-shifted and down-shifted from the incident x-ray energy, and an unshifted Rayleigh peak. The unshifted Rayleigh peak is a result of elastic scattering of incident radiation by electrons that are tightly bound and electrons that dynamically follow the ion motion. The plasmon energy shift is directly related to the electron density. For small values of \mathbf{k} , i.e. large values of α , the density can be calculated using the Bohm-Gross relation [23, 24], an analytical expansion of the dispersion relation,

$$\omega_{pl}^2 = \omega_p^2 + 3k^2 v_{th}^2 (1 + 0.088 n_e \Lambda_e^3) + \left(\frac{\hbar k^2}{2m_e} \right)^2 \quad (6)$$

where $v_{th} = \sqrt{k_B T / m_e}$ is the thermal velocity and $\Lambda_e = h / \sqrt{2\pi m_e k_B T}$ is the thermal wave length. In Eq. (6), the first term is the plasma frequency ($\omega_{pl} = n_e e^2 / \epsilon_0 m_e$)^{1/2} that results from electron oscillations in the plasma [25] and is only dependent on the electron density, n_e . Here, ϵ_0 the permittivity of free space, e is the electron charge, and m_e is the electron mass. The second term represents the effect on propagation of the oscillations from thermal pressure [23]. The third term includes degeneracy effects from Fermi pressure [26], and the last term is the quantum shift, calculated from the Compton energy, $E_C = (\hbar/2\pi)^2 k^2 / 2m_e = 9.3 \text{eV}$ for this experiment. Here, h is Planck's constant and k , Eq.(5), is dependent on the probe energy and scattering angle.

For conditions in this experiment, thermal corrections to the dispersion relation due to the propagation of oscillations are small, and the quantum shift and electron

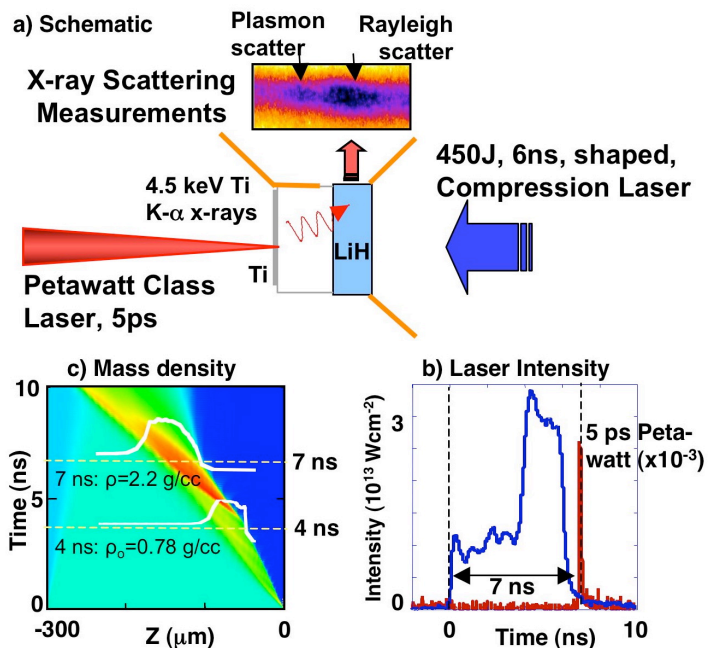


FIG. 1: a) Schematic of the experimental configuration. A ultrashort (10 ps), mono-energetic ($\Delta E/E < 0.3\%$), K- α x-ray probe is generated via ultra short-pulse laser irradiation of a titanium foil. The x rays interact with matter that is compressed by a nanosecond-long shaped laser pulse. The x-ray Thomson scattering spectrum shows inelastic scattering on plasmons and elastic Rayleigh scattering features. b) Waveforms of the compression (blue) and probe (red) laser beams. The shaped compression beam drives a slow intensity shock into the LiH with a low intensity foot ($1 \times 10^{13} \text{Wcm}^{-2}$) followed by a stronger shock with a higher intensity peak ($3 \times 10^{13} \text{Wcm}^{-2}$). The evolution of the shocks is measured at various times by changing the delay between the short pulse probe laser and the long-pulse pump beam. c) Radiation hydrodynamic modeling indicates coalescence of the shock waves at $t = 7$ ns from the launch of the compression beam.

oscillations account for most of the measured plasmon shift relative to the unshifted Rayleigh peak. Therefore, the plasmon frequency provides a sensitive measure of the plasma electron density.

EXPERIMENT

The experiment was performed at the Titan laser facility [27] where a long pulse beam was used to compress the solid density LiH targets ($1.9 \times 3 \times 0.3$ mm, $\rho_0 = 0.78 \text{g/cc}$) and a second short-pulse beam was used to produce probe x-rays from a solid density foil. The shaped long-pulse drive beam (450 J, 527 nm, 2ω) compressed the LiH targets by launching two planar shocks into the material with an intensity of $I = 1 \times 10^{13} \text{W/cm}^2$ in a 4 ns long foot, followed by an intensity of $I = 3 \times 10^{13} \text{W/cm}^2$ in

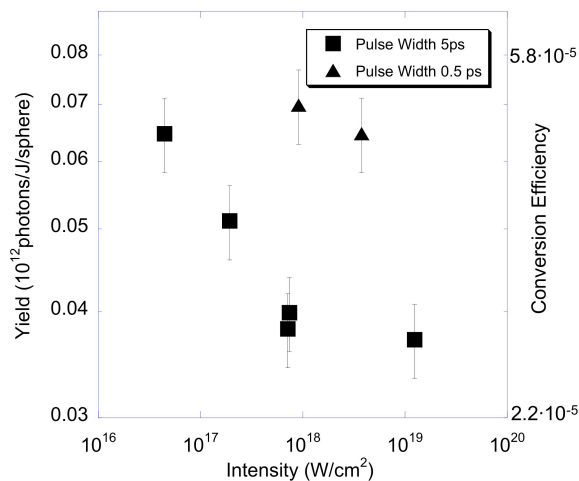


FIG. 2: Conversion efficiency of laser energy into Ti K-alpha radiation as a function of varying short-pulse probe laser intensity. Conversion efficiencies for a pulse width of 0.5 ps were comparable to that of 5 ps pulse widths, but the latter was used due to restrictions on available laser energy for a 0.5 ps laser pulse width.

a 2 ns long high intensity peak, see Fig 1 b). A 600 μm phase plate was used to create a smooth drive beam intensity profile. Nearly mono-energetic Ti K- α x-rays ($\Delta E/E = 0.3\%$) were produced using intense short-pulse laser irradiation (300 J, 1053 nm, 5 ps) of a 10 μm thick Ti foil. Hot electrons created in the laser-solid interaction produce emission from the cold solid density bulk of the foil via K shell ionization of neutral or weakly ionized atoms.

Figure 1 c) shows a calculated mass density contour as a function of target thickness and time. The time $t=0$ denotes the start of the long-pulse drive beam. This calculation used the experimental long-pulse drive beam waveform and a 1D Lagrangian radiation-hydrodynamic modeling code HELIOS [30]. The results were only weakly dependent on the details of radiation transport and heat conduction. Calculations indicated shock coalescence at about 7 ns after the start of the long-pulse beam and compression of about three times solid density at coalescence. This experiment was designed to probe these conditions.

The targets and Ti source foils were mounted on photo-structurable glass holders along with gold shields (10 x 7.5 x 0.025 mm) to block the view of the source and blow-off plasmas to the scattering spectrometer. The holders restricted the view of the source x-rays to the LiH, with a solid angle of 1.6×10^{-1} sr. Scattered radiation was observed side-on to the LiH targets at a scattering angle of $40 \pm 10^\circ$ with a Highly Oriented Pyrolytic Graphite (HOPG) spectrometer. See Fig. 1 a) for a schematic of the experiment.

The Titanium K- α line was chosen for scattering due to its small bandwidth ($\Delta E/E = 3 \times 10^{-3}$) and suffi-

cient conversion efficiency. For scattering in the collective regime, a small bandwidth and lack of satellites on the red wing are advantageous for high resolution of the downshifted plasmon peak, shifted in energy about 24 eV. Also, the moderate energy allows the possibility for collective, as well as non-collective, scattering while allowing sufficient penetration through shock compressed targets, with an attenuation length of about 470 μm .

To detect the scattered x-rays, a Bragg spectrometer with a large curved Highly Oriented Pyrolytic Graphite (HOPG) crystal (24 x 70 mm) was used in the van Hamos geometry [28, 29] and mosaic focusing mode. The scattered light was then diffracted with high spectral resolution onto an Imaging Plate (IP) detector. Here, the source-to-crystal and crystal-to-detector distances were set to the focal distance, $F=R/\sin(\theta_B)$, where R is the radius of curvature of the HOPG crystal and θ_B is the Bragg angle. For second order Bragg diffraction and a radius of curvature of 11.5 cm, the focal distance was about 13.1 cm. To moderate the amount of hot-electron driven fluorescence from materials near the crystal, the HOPG crystal was mounted on a plastic stalk. Imaging Plate detectors with a resolution of 25 μm (corresponding to 0.33 eV in this experiment) were used to record images of the scattered radiation, see Fig 1 a). To filter noise and background from bremsstrahlung, 25 μm thick Be foils covered the IP detectors.

Due to the small cross section for Thomson scattering ($6.65 \times 10^{-25} \text{cm}^2$) and short lifetime of the probe emission, it was necessary to optimize conditions to produce a high number of photons for single shot accuracy. The conversion efficiency (C.E.) of laser light for the production of x rays was investigated by varying the short pulse beam focus and pulse duration, see Fig. 2. Here, an increase in conversion efficiency with increasing laser spot size, i.e. decreasing intensity, was observed. Also, a defocused beam results in lower background from bremsstrahlung radiation. A high conversion efficiency of 5×10^{-5} , was achieved at a laser intensity of $9 \times 10^{17} \text{W/cm}^2$ for a pulse width of 0.5 ps. However, restrictions on the laser system limited the available energy for pulse widths of 0.5 ps to half of the energy available for a pulse widths of 5 ps. Therefore, scattering data were taken with a defocused short-pulse beam spot size of 400 μm and a pulse width of 5 ps ($4 \times 10^{16} \text{W/cm}^2$), resulting in approximately 6×10^{10} photons/J/sphere and a conversion efficiency of 5×10^{-5} .

The scattering volume seen by the spectrometer (0.1 x 0.4 x 0.3 mm) was mainly restricted by shields and the material transmission, with a measured attenuation length of 470 μm . The low transmission of the LiH targets compared to a tabulated attenuation length of 7350 μm [31] is attributed to impurities ($< 2\%$) in the sample and a thin oxide layer of $< 20 \mu\text{m}$. For the case of unheated LiH, it was estimated that of the 2×10^{13} generated photons, 3×10^{11} photons reached the scattering

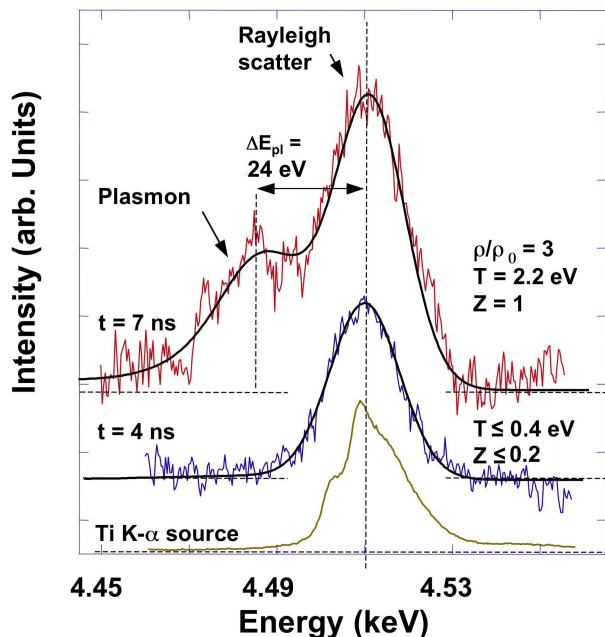


FIG. 3: Measured x-ray scattering spectrum from shocked LiH, showing elastic Rayleigh scattering and inelastic plasmon scattering features, with theoretical fits to the experimental data. At $t = 7$ ns (top), the plasmon energy shift of 24 eV indicates 3x compression, while the intensity of the elastic scattering feature shows heating to temperatures of 2.2 eV. Earlier in time, before the launch of the second strong shock ($t=4$ ns), elastic scattering is mainly observed (middle), as demonstrated when compared with the K- α source spectrum (bottom). The observation of plasmons at $t = 7$ ns indicates the transition to the metallic free electron plasma in solid density LiH.

target and approximately 8×10^8 photons scattered elastically. The solid angle of the spectrometer crystal was approximately 1.6×10^{-3} sr, with a view of 0.53 radians in the non-dispersive plane and an integrated reflectivity of 3 mrad in the dispersive plane due to the mosaicity of the crystal. Of the 8×10^8 scattered photons, an estimated 10^5 were collected by the HOPG spectrometers, consistent with the measured signal strength for scattering from uncompressed LiH targets.

RESULTS AND DISCUSSION

Experimental scattering spectra at shock coalescence ($t = 7$ ns) and just before the launch of the second strong shock wave ($t = 4$ ns) are shown in Fig. 3. Also shown is the Ti K- α source spectrum measured with the HOPG spectrometer that showed no spectral features on the red wing and a bandwidth of $\Delta E/E = 0.3\%$, advantageous for the observation of plasmons. Thomson scattering data at shock coalescence ($t = 7$ ns) show inelastic and elastic scattering features from interaction with free

and bound electrons. The free (delocalized) electrons undergo plasma (Langmuir wave) [25] oscillations at the plasma frequency, yielding the collective plasmon scattering feature [11], while scattering from bound electrons and electrons that dynamically follow the ion motion results in an elastic Rayleigh scattering component. The ionization potentials of tightly bound Li and H K-shell electrons are greater than the Compton energy and are not excited from interaction with the x-rays.

At $t=4$ ns, the lack of strong inelastic scattering indicates that there are little or no free electrons and scattering is dominated by elastic scattering. Theoretical fits to the scattering data that account for scattering from free, bound, and weakly bound electrons poses an upper limit on the degree of ionization, $Z^* < 0.2$. An increase in the elastic scattering intensity compared to scattering from unheated LiH targets of $40\% \pm 10\%$ indicates temperatures of < 0.4 eV.

Scattering data at $t=7$ ns when the shock waves coalesce, show strong inelastic scattering from plasmon oscillations that are downshifted from the elastic scattering feature by $\Delta E_{pl} = 24$ eV. In these data, the elastic scattering signal increased by $100\% \pm 10\%$ compared to cold scattering from unheated samples, indicating a temperature of 2.2 eV. Heating and compression of the material results in an ionization state of $Z^*=1$ for Li(+)-H. The ionization is determined from the shape and intensity of the inelastic scattering peak with an error of $\pm 10\%$ in theoretical fitting to the experimental data. The shift of the plasmon peak provides an accurate measure of the electron density, see Eq. (6) for an analytical expansion of the dispersion relation, which yields the material compression for known ionization state. The electron density, $n_e = 1.7 \times 10^{23} \text{cm}^{-3}$, was determined from the shift of plasmon frequency relative to the elastic peak (4.51 keV) with 10% error due to noise. For conditions in this experiment, correction to the dispersion relation due to thermal motion of the electrons was negligible, providing an accurate measure of the electron density.

The intensity of the elastic scattering feature is dependent on the number of electrons that dynamically follow the ion motion and the ion-ion structure factor, which is dependent on the ion temperature. Therefore, the ion temperature can be inferred from the elastic scattering intensity. The plasma screening length for this degenerate system is approximately $\lambda_S = 0.57 \text{\AA}$, and approaches the Thomas-Fermi length. In this case the collective regime is accessed, with a collective scattering parameter of $\alpha = 1.1$ (Eq.(3)), and the scattering length is on the order of the screening length required to observe plasmon oscillations.

Plasmon scattering at shock coalescence indicates a dense metallic plasma state. Density Functional Theory (DFT) calculations [34] also predict metallic properties for the material density and temperature conditions at coalescence, consistent with the measurement of plas-

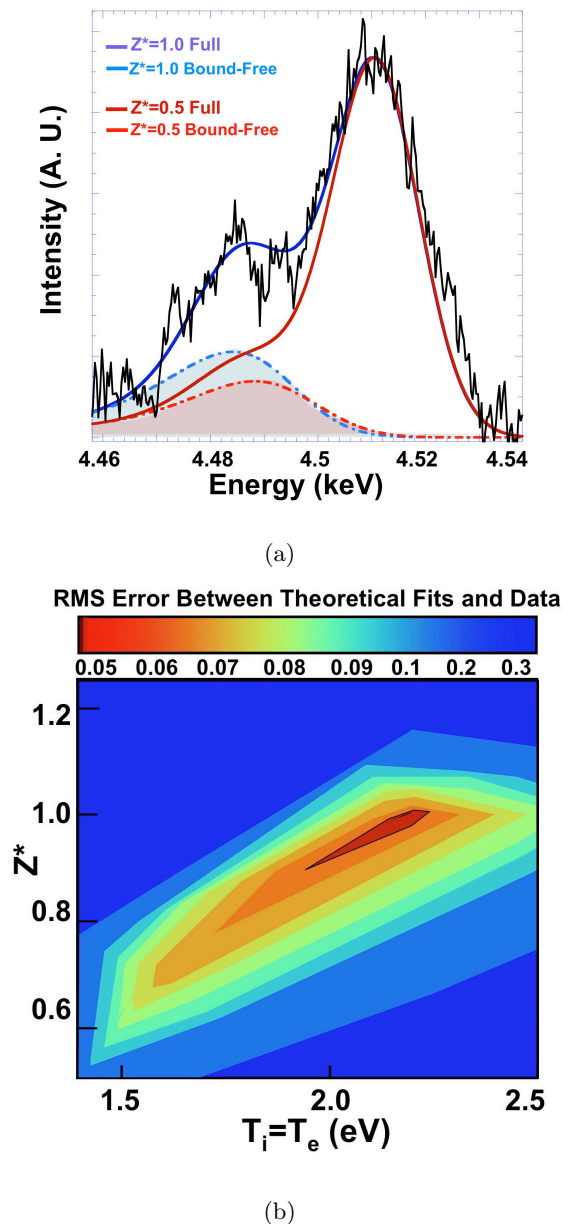


FIG. 4: a.) Experimental scattering of Ti K-alpha from compressed LiH, 7ns after the first of two shocks was launched into the solid density target, with simulated theoretical spectra. Sensitivity of ionization state changes in the theoretical fit to the experimental data is shown with the best fit (blue) with $Z^*=1$, compared to fits with $Z^*=0.5$ (red). Here, the temperature and density, 2.2 eV and $1.7 \times 10^{23} \text{ cm}^{-3}$, respectively, are held constant. b.) Sensitivity of theoretical fits to the experimental spectra for varying temperatures and ionization states, Z^* . Root Mean Squared (RMS) differences are color coded for given temperature and Z^* combinations, where the centered dark red island is a range of possible best fits. The error of this fitting method to the experimental data is $\pm 10\%$ for the ionization state Z^* .

mons. These calculations estimate two orders of magnitude increase in the DC conductivity for the compressed case, $4.3 \times 10^5 / \Omega \text{ m}$, approaching the conductivity of a typical metal, compared to the conductivity at standard-temperature-pressure (STP) conditions, $1.4 \times 10^3 / \Omega \text{ m}$.

Theoretical fits to the experimental data are obtained using multiple-species ion-ion structure factors from screened-one-component electron-ion interaction potentials [32]. The theoretical model used to calculate the electron-electron structure factor employs the Random Phase Approximation (RPA). Corrections to the electron-electron structure factor due to local field corrections (LFC) to the bare coulomb interaction potential, that satisfies the compressibility sum rules in the long wavelength limit ($k \rightarrow 0$) accessed by collective scattering, the LFC is negligible and the electron structure factor reduces to the linearized Debye-Hückel approximation [35]

$$S_{ee}(k) = k^2 / (k^2 + (1/\lambda_S)^2). \quad (7)$$

From the screening length for a partially degenerate electron fluid, the electron-electron structure factor, $S_{ee}(k = 1.6 \text{ \AA}^{-1}) = 0.46$, can be determined from its dependence on the electron density, approaching the structure factor for a completely degenerate plasma, $S_{ee}(k = 1.6 \text{ \AA}^{-1}) = 0.45$. With this value for the electron-electron structure factor and the experimental intensities of the elastic and inelastic scattering components, the ion-ion structure factor can be inferred. Since the ions are non-degenerate, the screening length in Eq.(7) can be approximated by the Debye-Hückel length, resulting in $S_{ii}(f+q)^2(k = 1.6 \text{ \AA}^{-1}) = 0.71$, and the ion temperature can be obtained. To fit the data, a more sophisticated model was used that applies strong coupling (ion sphere model) and screening corrections (linear screening approximation) to the ion-ion structure factor, resulting in $S_{ii}(f+q)^2(k = 1.6 \text{ \AA}^{-1}) = 0.54$ [32]. This model has been tested in new separate experiments on compressed LiH with similar density and temperature conditions [36]. Data in those experiments show screening effects that are consistent with the models applied in Fig. 3.

Figure 4 a) shows sensitivity of the scattering data to ionization state, Z^* , at 7ns after the launch of the first shock. The ionization state is sensitive to the relative intensity of inelastic to elastic scattering, as well as the shape of the inelastic scattering feature. The shaded region in Fig. 4 a) is the scattering contribution from bound-free scattering, adding to the inelastic scattering feature. For a decrease in the ionization state at a fixed electron density, the ratio of elastic to inelastic scattering increases due to an increase in the amount of Rayleigh scattering from having a greater density of neutral Li and H atoms. For ionization states greater than one per LiH molecule, the H atom becomes ionized, with an ionization potential greater than the Compton energy. Then,

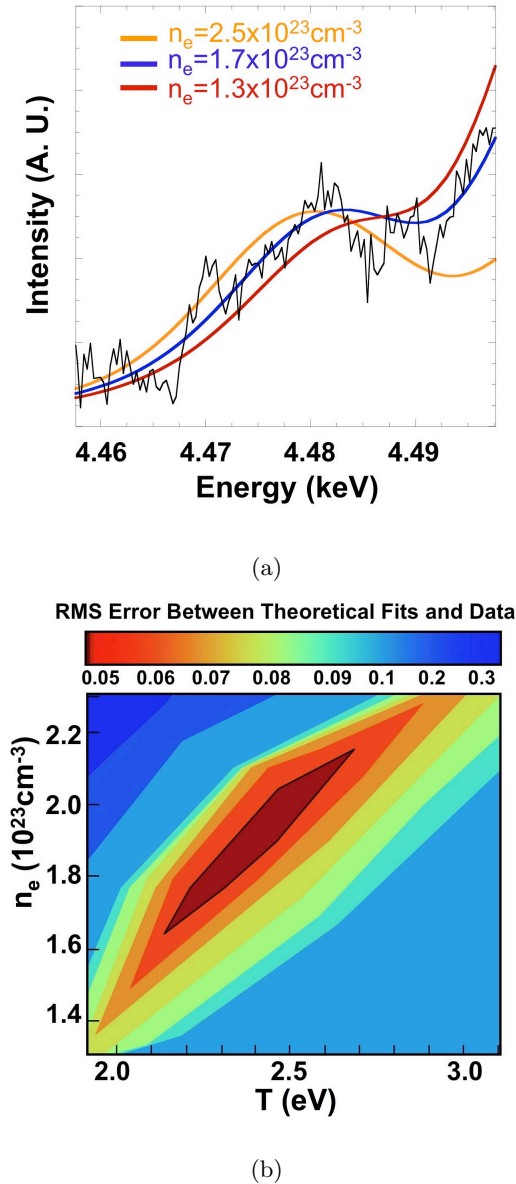


FIG. 5: a.) Experimental scattering of Ti K-alpha from compressed LiH, 7ns after the first of two shocks was launched into the solid density target, with simulated theoretical spectra. Sensitivity of density changes in the theoretical fit to the experimental data is shown with the best fit (black) at $1.7 \times 10^{23} \text{cm}^{-3}$, compared to fits at $1.3 \times 10^{23} \text{cm}^{-3}$ and $2.5 \times 10^{23} \text{cm}^{-3}$ (blue and green curves). Here, the temperature and ionization state, 2.2 eV and $Z^* = 1$, respectively, are held constant. b.) Sensitivity theoretical fits to the experimental spectra for varying temperatures ($T_e = T_i$) and electron densities. Root Mean Squared (RMS) values are color coded for given temperature and density combinations, where the centered black island is a range of possible best fits. The error of this fitting method to the experimental data is about $\pm 10\%$ for temperature and electron density.

the ratio of elastic to inelastic scattering increases mainly as a result of a decrease in bound-free scattering from fewer neutral hydrogen atoms. The bound-free term was calculated using hydrogenic wave functions which can pose a systematic error in the determination of Z^* for ions with many bound electrons and is subject to future studies with more advanced models [37]. However, an ionization state of $Z^* = 1$ for this experiment is also estimated from radiation-hydrodynamic modeling, in agreement with analysis from the shape of the inelastic feature, demonstrating sensitivity to Z^* . Thermal excitation of the 1s Li and H electrons is negligible for the low electron temperature < 3 eV in this experiment, whereas the weakly bound 2s Li electron is predicted to be free due to continuum lowering. Since temperature is also sensitive to the relative intensity of the plasmon and Rayleigh scattering feature, a range of possible best fits for various temperatures and ionization states provided upper and lower bounds for Z^* . Root Mean Squared (RMS) values of theoretical fitting to the experimental data are shown in Fig. 4 b) providing Z^* within $\pm 10\%$.

Figure 5 a) shows sensitivity of the plasmon frequency shift to electron density at 7ns after the launch of the first shock into the target. As the electron density increases, the shift of the plasmon frequency increases as expected from the dispersion relation. Figure 5 b) shows RMS differences between theoretical fitting to the experimental data for a range of temperatures and densities, since the ratio of elastic to inelastic scattering is dependent on ion density and temperature. The dark-colored island in the center of the plot indicates best theoretical fitting with 10% error in the temperature and electron density. Sensitivity of theoretical fits to the experimental data for density, ionization state, and temperature show that these parameters can be determined simultaneously for single shot characterization.

Measured temperatures as a function of time are shown in Fig. 6 a), providing temperature evolution during shock progression. Fig. 6 a) also includes radiation-hydrodynamic calculations using the 2D Lagrangian code LASNEX [38]. The strong increase in temperature at 7 ns indicates shock wave coalescence. Errors in the temperature, 10-20%, is mainly due to noise in single shot data for lower scattering signals. Partial scattering from uncompressed material has been taken into account, resulting in a correction of about 10%. The range of calculated temperatures is a result of variations in the amount of impurities and oxide layer thickness, consistent with target characterization. The radiation-hydrodynamic modeling used the experimentally measured laser pulse shape and irradiance. Laser absorption in the target was estimated using an inverse bremsstrahlung model and the simulations included radiation transport. The main dependency of the simulation results is on the choice of the EOS and is rather insensitive to details in radiation transport and heat conduction. Sensitivity of theoretical

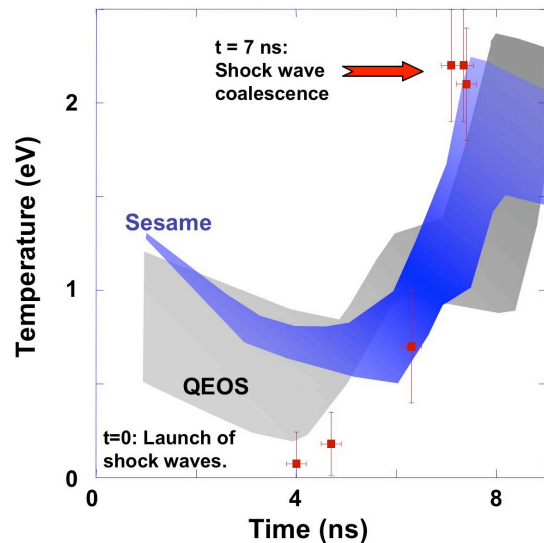
fitting to the experimental data for varying temperature is shown in Fig. 6 b) where the elastic scattering intensity increases with increasing temperature due to its dependence on the ion-ion structure factor.

The Quotidian Equation of State (QEOS) [12] is based on a model that includes modified electronic Thomas-Fermi statistics with the ion thermal motion calculated beyond the Grüneisen EOS by including temperature-dependent corrections to the pressure. This model shows consistency with the wide range of temperatures accessed in this experiment. Calculations using the Sesame EOS includes atomic structure based on solutions of the single particle quantum levels in the self-consistent field of an atom [39]. The peak temperature and experimentally observed coalescence time are in excellent agreement with modeling that uses the Sesame EOS. However, early in time the agreement is less satisfactory indicating that future comparisons with first-principle statistical models [40] will be useful to understand these weakly shocked systems.

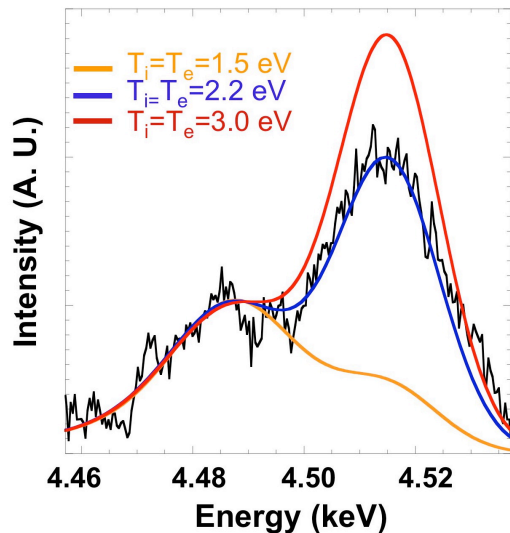
At peak temperature and density conditions, calculations indicate pressures in the range of $P = 300 - 420$ GPa. With $Z^* = 1$ and the measured electron density from the plasmon frequency shift, we determine a mass density of $\rho = 2.25$ g/cc at shock coalescence, a factor of three times solid density compression. This value is consistent with EOS data obtained from density functional perturbation theory [41], and approaches conditions where a pressure induced insulator-metal transition is predicted [42]. Here we measure the metallic state from the observation of plasmons at shock coalescence. This transition is thought to occur simultaneously with a structural transition from the B1 NaCl like phase to the B2 CsCl like phase, which has been previously observed in all other alkali-hydrides except LiH [43]. Wang et. al [42] predicts that the B1 to B2 transition occurs at 313 GPa, simultaneously with the MIT transition that is a result of the estimated near zero band gap energy in the B2 phase. However, DFT calculations that account for underestimation of the band gap energy using the Local Dynamic Approximation (LDA) predict that the MIT should occur first, followed by the B1 to B2 transition at 308 GPa [41]. Future experiments using x ray Thomson scattering to measure the B1 to B2 transition and the MIT transition in more detail would provide insight into the structural behavior of LiH under extreme pressure conditions, as well as other materials of interest.

CONCLUSIONS

In summary, we have successfully obtained experimental K- α X-ray Thomson scattering data, enabling 10 ps temporal resolution for characterization of shock compressed, solid density matter. The spectral properties of Ti K- α , ie. moderate energy and small bandwidth,



(a)



(b)

FIG. 6: a.) The temperature of the shocked LiH as function of time, where $t=0$ denotes the start of the compression beam, from x-ray Thomson scattering measurements (red) and from radiation-hydrodynamic modeling using different EOS models. The range of temperatures plotted for each model accounts for LiOH surface impurities (lower bounds) to no impurities (upper bounds). The experiments and calculations demonstrate efficient heating by shock coalescence with small differences in shock timing that can be resolved with the short K- α x-ray pulses. b.) Sensitivity of theoretical fitting to the experimental data for varying temperature. The intensity of the elastic scattering feature increases with increasing temperature, from dependence on the ion-ion structure factor.

are well suited for collective scattering from plasmons. A transition to the dense metallic plasma state in solid density material has been shown, resulting in the observation of plasmons. This has allowed testing of radiation-hydrodynamic calculations utilizing different EOS models for dense shocked matter. This technique is opportune for inertial confinement fusion experiments, such as the National Ignition Facility [44], that will achieve extreme density conditions and require high temporal resolution for characterization of short lived states of compression, and can be used to test radiation hydrodynamic models. We further show that K- α scattering can provide a sufficient source, with $\sim 10^{12}$ photons on target, for pump-probe experiments and diagnosing warm dense matter in laboratory astrophysics experiments.

ACKNOWLEDGMENTS

This work was performed under the auspices of the U.S. Department of Energy by Lawrence Livermore National Laboratory under Contract DE-AC52-07NA27344. This work was further supported by DOE grant, NA-16 Intermediate Facility Initiative, by grants 08-ERI-002, 08-LW-004, and the Lawrence Scholar Program (LSP) fellowship.

-
- [1] H. C. Connolly and Jr., Stanley G. Love, *Science* **280**, 62 (1998).
- [2] T. Guillot, *Science* **286**, 72 (1999).
- [3] N. C. Holmes, M. Ross, and W. J. Nellis, *Phys. Rev. B* **52**, (1995).
- [4] G. W. Collins *et al.*, *Science* **281**, 1178 (1998).
- [5] M. D. Knudson, D. L. Hanson, J. E. Bailey, C. A. Hall, and J. R. Asay, *Phys. Rev. Lett.* **87** (2001).
- [6] C. P. McKay and William J. Borucki, *Science* **276**, 390 (1997).
- [7] J. D. Lindl *et al.*, *Phys. Plasmas* **11**, 339. (2004).
- [8] C. P. J. Barty *et al.*, *Nucl. Fusion* **44**, S266 (2004). J. D. Zuegel *et al.*, *Fusion Science and Tech.* **49** 453-482 (2006).
- [9] A. L. Kritcher *et al.*, *Science* **322**, 69 (2008).
- [10] O. L. Landen *et al.*, *Rev. Sci. Instrum.* **72**, 627 (2001).
- [11] S. H. Glenzer *et al.*, *Phys. Rev. Lett.* **98**, 065002 (2007).
- [12] R. M. More, K. H. Warren, D. A. Young, and G. B. Zimmerman, *Phys. Fluids* **31**, 3059 (1988).
- [13] S. Crockett, SESAME 7246, in Los Alamos National Laboratory Report No. LA-UR-06-8403.
- [14] S. H. Glenzer *et al.*, *Phys. Plasmas* **6**, 2117 (1999).
- [15] G. Gregori *et al.*, *Phys. Plasmas* **11**, 2754 (2004). *ibid.*, *J. Quant. Spectrosc. Radiat. Transfer*, **99**, 225 (2006).
- [16] S. H. Glenzer *et al.*, *Phys. Rev. Lett.* **90**, 175002 (2003), *ibid* *Phys. Plasmas* **10**, 2433 (2003).
- [17] S. Tzortzakis, P. Audebert, P. Renaudin, *et al.* *J. Quant. Spectr. Trans.* **99**, 614 (2006).
- [18] J. Chihara, *J. Phys. F: Met. Phys.* **17**, 295 (1987).
- [19] J. Chihara, *J. Phys. : Condens. Matter* **12**, 231 (2000).
- [20] C. Kittel, *Introduction to Solid State Physics*, 7th Ed., Wiley, (1996).
- [21] F. Perrot and M.W.C. Dharma-wardana, *Phys. Rev. B* **62**, 16536 (2000).
- [22] G. Gregori, S. H. Glenzer, W. Rozmus, R. W. Lee, and O. L. Landen, *Phys. Rev. E* **67**, 026412 (2003).
- [23] D. Bohm and E. P. Gross, *Phys. Rev.* **75**, 1851 (1949).
- [24] R. Thiele *et al.*, *Phys. Rev. E* **78**, 026411 (2008).
- [25] L. Tonks and I. Langmuir, *Phys. Rev.* **33**, 195 (1929).
- [26] R. Zimmerman, *Many-Particle Theory of Highly Excited Semiconductors* (Teubner, Leipzig, 1987).
- [27] P. Beiersdorfer, *et al.*, NIFS Proceedings Series No. NIFS-PROC-57, p. 40-46 (2004).
- [28] F. J. Marshall and J. A. Oertel, *Rev. Sci. Instrum.* **68**, 735 (1997).
- [29] M. K. Urry, G. Gregori, O. L. Landen, A. Pak, and S. H. Glenzer, *J. Quant. Spectr. Rad. Trans.* **99**, 636 (2006).
- [30] J. J. MacFarlane, I. E. Golovkin, P. R. Woodruff, *JQSRT* **99**, 381-397 (2006).
- [31] B. L. Henke, E. M. Gullikson, and J. C. Davis, *ADNDT*, **54** 181 (1993).
- [32] G. Gregori, A. Ravasio, A. Hill, S. H. Glenzer, and S. J. Rose, *High Energy Den. Phys.* **3**, 99 (2007).
- [33] J. Sheffield, *Plasma Scattering of Electromagnetic Radiation* (Academic Press, New York, 1975).
- [34] B. Holst, R. Redmer, and M. P. Desjarlais, *Phys. Rev. B* **77**, 184201 (2008).
- [35] P. Debye and E. Huckel, *Phys Z* **24** , 185 (1923).
- [36] A. L. Kritcher, *et al.*, *in Progress*, (2009).
- [37] S. Sahoo, G. F. Gribakin, G. Shabbir Naz, J. Kohanoff, and D. Riley, *Phys. Rev. E* **77**, 046402 (2008).
- [38] G. B. Zimmerman and W. L. Kruer, *Comments Plas. Phys.* **2**, 51 (1975).
- [39] D. A. Lieberman, *Phys. Rev. B* **20**, 4798 (1979).
- [40] T. Ogitsu, E. Schwegler, F. Gygi, and G. Galli, *Phys. Rev. Lett.* **91**, 175502 (2003).
- [41] W. Yu, C. Jin, A. Kohlmeier, *J. Phys. Condens. Matter* **19**, 086209 (2007).
- [42] Y. Wang, R. Ahuja, and B. Johansson, *Phys. Stat. Sol.* **235**, 470 (2003).
- [43] S. J. Duclos, Y. K. Vohra, A. L. Ruoff, S. Filipek, and B. Baranowski, *Phys. Rev. B* **36** 7664 (1987).
- [44] E. Moses, C. R. Wuest, *Fusion Sci. Tech.* **47**, 314-322 (2005).
- [45] E. Funfer *et al.*, *Phys. Lett.* **5**, 125 (1963).
- [46] H. J. Kunze *et al.*, *Phys. Lett.* **11**, 42 (1964).